Synthesis of Fe/Mg-doped NMC6 22 from Spent Nickel Catalyst as Lithium-Ion Battery Cathode

Endah Retno Dyartanti[1,2,*] , *Agnestasia Milenia Putri* Kurniawan[1] , and *Arifiah Muflikhati* Putri[1]

[1]Department of Chemical Engineering, Faculty of Engineering, Universitas Sebelas Maret, Surakarta 57126, Indonesia
[2]Centre of Excellence for Electrical Energy Storage Technology, Universitas Sebelas Maret, Surakarta 57146, Indonesia

Abstract. The co-precipitation approach, along with nickel-rich (NMC622) cathode materials, magnesium, and Fe doping, was used to produce nickel-rich NMC (NMC622) cathode materials from spent nickel catalysts. Both X-ray diffraction (XRD) and Fourier transform infrared spectroscopy (FTIR) were utilized in order to carry out the characterization of the NMC622 materials. The structural study showed that the doped materials had a structure that was equal to that of $Li[Ni_{0,6}Mn_{0,2}Co_{0,2}X_y]O_2$, which has a layered hexagonal structure similar to that of α-$NaFeO_2$. The electrochemical test found that Mg 1 mol% had the highest discharge capacity at 99.61 mAh/g. This was determined by the results of the test. The use of magnesium as a dopant in structurally stable, Ni-rich NMC materials led to an increase in the electrochemical capacity of the Mg-doped NMC. Magnesium exhibited a significant amount of potential as a dopant. It is necessary to do additional research into the functional testing of magnesium as a doping material in order to maximize its use for a longer cycle life and improved thermal stability lithium ion batteries.

1 Introduction

In the current modern period, electrical equipment continue to change and advance. The need for lithium batteries at an affordable price has grown as the electric car sector has developed [1]. The lithium-ion battery is one of the growing batteries today. Electric energy storage needs to advance since it needs to be portable, effective, and have good performance [2]. Therefore, the battery assembly must have an active component that satisfies market requirements.

The nickel-rich oxide layer ($LiNi_xM_{1-x}O_2$, x>0,5) is currently the choice as a high-energy cathode materials for lithium-ion batteries, and the combined capacity is more than 200 mAh/g when active at high voltage 4 V vs Li/Li^+ [3]. In the industrial world, nickel is a substance that is employed in metallurgy as well as serving as a catalyst in operations like hydrogenation, hydrodesulfurization, hydrorefining, and methanation [4]. [1]Chemical capabilities in nickel catalysts that have undergone industrial operations may be diminished. However, researchers are currently developing a variety of techniques to restore the ability

* Corresponding author: endah_rd@staff.uns.ac.id

of nickel, one of which is the hydrometalurgical method using organic or inorganic acids as lindiic acid to recover metals as well as battery waste [5].
One promising Ni-rich cathode is cathode because of its high theoretical capacity (~200 mAh/g), environmentally friendly, and can reduce production costs [6]. The widely marketed $LiNi_aMn_bCo_cO_2$ (where a+b+c = 1) materials have different Ni, Mn, and Co mol comparisons respectively $LiNi_{0.33}Mn_{0.33}Co_{0.33}O_2$ (NMC333), $LiNi_{0.5}Mn_{0.3}Co_{0.2}O_2$ (NMC532), $LiNi_{0.6}Mn_{0.2}Co_{0.2}O_2$ (NMC622), $LiNi_{0.8}Mn_{0.1}Co_{0.1}O_2$ (NMC811), etc. At the same voltage, NMC622 is more preferable than other material (NMC532) because it has a greater specific capacity and better rate capability [7].
However, NMC materials still have a barrier to poor capacity and voltage weakening when exposed to high operating voltage during charging/discharging. This creates some problems in the practical application of the lithium battery market [8]. These deficiencies can be eliminated by making various modifications, such as surface coating, cation doping, heterostructure, and core-shell structure. Among the modifications that have been developed, cation doping is considered a relatively simple and easy-to-operate approach to enhancing the electrochemical properties of the NMC cathode [9].
Better NMC materials have been developed via extensive work in both the academic and industrial sectors. Doped NMCs displayed improved thermal stability than pristine [10] on NMC622 material using co-precipitation method with Mg and Zr doping. The rate of change differed depending on %mol dopant and calcination temperature. Previous study on $LiNi_{1/3}Co_{1/3}Mn_{1/3}Fe_x(OH)_2$ made using hydroxide co-precipitation and Fe as a doping element from spent batteries [11]. Fe can be more easily extracted leach liquors due to Fe's favorable impacts on the electrochemical and thermal properties of NMC. Mg also used in $LiNi_{0.84}Co_{0.11}Mn_{0.05}O_2$ and consequenced 1 wt% Mg-doped offers a high discharge capacity of 196.7 mAh g 1 (0.1 C) and retains the capacity retention of 85.95% after 80 cycles, suggesting exceptional cycling performance [12]. The Mg-doped samples also outperform the un-doped sample in terms of electrochemical performance at high cut-off voltage. The manufacture of NMC materials from spent nickel catalysts showed coulombic efficiency and sampling capacity retention were >98% and 87,18% respectively after 50 cycles which were fairly comparable to commercial NMC in terms of stability [5].
In this study, due to its higher specific capacity, NMC622 is the ratio employed in the acid leaching process to synthesize Ni-rich NMC material from spent nickel catalyst. Fe and Mg are used as dopants to stabilize NMC622 material synthesized through co-precipitation processes due to the common and abundant presence of such materials.

2 Materials And Methods

Materials used are spent nickel catalyst from PT. Petro Oxo Nusantara (Indonesia), Magnesium sulfat, *Cobalt* sulfat, and doping material: $FeSO_4.7H_2O$ from Merck (Germany) and $MgSO_4.6H_2O$ from Riedel-de Haen (Germany). Additional material are $HOC(CH_2CO_2H)_2$, H_2O_2, $H_2C_2O_4$, NaOH, styrene butadiene rubber (SBR), sodium carboxyl methyl cellulose (CMC), acetylene black (AB), aquadest, and Litium hidroksida (Leverton, US).

2.1 Synthesis of nickel citrate [$Ni_3(C_6H_5O_7)_2$]

The leaching process is by mixing the nickel spent catalyst and 1 M citric acid solution in a ratio of 1 : 5 to the volume of citric acid at a temperature of 80 °C and at a rate of 600 rpm for 3 hours. H_2O_2 was added as a reducing agent for 3% of the volume of citric acid. The leaching process results are then filtered and used for the NMC precursor synthesis process.

2.2 Synthesis of NMC precursor

The manufacture of the NMC precursor is carried out by the co-precipitation method at a temperature of 60 °C with a melting rate of 600 rpm for 2 hours. The co-precipitation process is carried out by mixing the leaching reaction filter with $MnSO_4.H_2O$, $CoSO_4.7H_2O$, $FeSO_4.7H_2O$, or $MgSO_4.6H_2O$ in sequence. The addition follows the mol ratio Ni: Mn: Co: Fe or Mg = (0,6-y): 0,2: 0,2: y as in Table 1. Then, the process of coprecipitation of the solution will gradually lower its pH. First, add the NaOH 5 M solution to pH 4. The solution will then be lowered to pH 2 using the 5 M oxalate acid solution [13]. The result of the copresipitation process is then inhabited, so that natural sedimentation or separation occurs based on the phase between liquid and solid. The solid (precipitate), which is a precursor, is filtered and washed with water to pH 7. The precursor is dried for 12 hours at a temperature of 100 ºC in the oven.

Table 1. Composition of Materials in The Co-precipitation Process

Sample	$Ni_3(C_6H_5O_7)_2$ (%mol)	$MnSO_4$ (%mol)	$CoSO_4$ (%mol)	$FeSO_4$ (%mol)	$MgSO_4$ (%mol)
Pristine	60%	20%	20%	-	-
Fe 1%	59%	20%	20%	1%	-
Fe 3%	57%	20%	20%	3%	-
Fe 5%	55%	20%	20%	5%	-
Mg 1%	59%	20%	20%	-	1%
Mg 3%	57%	20%	20%	-	3%
Mg 5%	55%	20%	20%	-	5%

2.3 Synthesis of $LiNi_{(0,6-y)}Mn_{0,2}Co_{0,2}X_yO_2$ (NMC-622)

The NMC622 synthesis process is carried out using the solid-state method. The precursor is added to $LiOH.H_2O$ and mixed using a mortar. Comparison of mol precursors : $LiOH.H_2O$ = 1: 1 Then the mixture is inserted into the muffle furnace for the formation of the NMC622. Calcination is carried out at a temperature of 500 °C for 6 hours in order to evaporate the oxalate components that are no longer needed. After that, sintering is carried out for 12 hours at a temperature of 900 °C. The blender aims to form the NMC622 material with heat without melting it so that it can be compressed well.

2.4 Material characterization

Nickel citrate solution resulting from leaching process characterized using Atomic Absorption Spechtrophotometry (AAS, Spectrometer iCE 3000 AA05022804 v1, 30 n). Both precursor and material of pristine NMC, Fe-doped and Mg-doped NMC were characterized using X-Ray Diffractometre to identify the crystalline phase in the materials using CuKα radiation material with λ = 1.5406 at 2θ and FTIR (Shimadzu FTIR Spectrometer, Japan) to identify functional groups of materials in the mid-IR region (4000-400 cm^{-1}). A performance test was conducted on the 18650-type cylindrical cell. The electrolytes, anodes, and

separators employed are lithium hexafluorophosphate ($LiPF_6$), cellgard, and graphite sheets. NMC622 are mixed with Acetylene Black (AB), Sodium Carboxyl Methyl Cellulose (CMC), Styrene Butadiene Rubber (SBR), and water until the slurry forms. The slurry is coated on a sheet of aluminum foil. After dryied in an oven set at 80 °C, the cathode sheet is put together to make a cylinder battery. The electrochemical test is analyzed using the NEWARE Battery Analyzer with charging up to a voltage of 4.25 V and then discharging until the voltage drops to 2.5 V.

3 Results and Discussion

3.1 Preparation of nickel nitrate

Spent catalysts, which serve as a source of nickel, first use a solution of citric acid at a temperature of 80 °C to produce a green-colored nickle citrate filtrate. Citric acid is chosen as a leaching agent because it has a good metal absorption efficiency based on a reference journal [14] with its optimal acid concentration at 1 M. The results of AAS analysis of samples of nickel citrate solution that have been made show that 1 M of citric acid is able to bind nickels as much as 14,3451 g/L so that the leaching efficiency reached >70%.

3.2 Analysis of precursor

The synthesis of NMC cathode materials begins with the formation of the NMC precursor through a mixture of nickel, manganese, and cobalt. The co-precipitation process was carried out by observing Li's leaching results with Mn and Co. Then doping with Fe and Mg, respectively, with variations of 1%, 3%, and 5% mol is also added during the co-precipitation process so that the precursor $Ni_{(0,6-y)}Mn_{0,2}Co_{0,2}X_y$ (X = Fe, Mg; y = 0.01, 0.03, 0.05) is formed.

XRD analysis of the NMC622 precursor with doping Fe or Mg is shown in Fig**.** 1. Based on Fig. 1, the doped precursor samples Fe and Mg had identical peaks with the pristine NMC622 samples. Previous research [10] revealed that the transitional metal oxalate $MC_2O_4.2H_2O$ [M = Ni, Mn, Co, Fe] crystallized in the α-monoclinic form with the spacegroup C2/c (for Mn) and the β-orthorhombic form with the Cccm spaceguard (for Ni, Co, Fe). Whereas $MgC_2O_4.2H_2O$ formed in distorted octahedralrhombic structure [15]. Precursor samples have peaks that are identical to the diphrase pattern of the β-orthorhombic shape. Individual phases of $NiC_2O_4.2H_2O$, $MnC_2O_4.2H_2O$, and $CoC_2O_4.2H_2O$ are missing in NMC-oxalate as a result of the homogenous mixing and dispersion of Ni-Co-Mn at the atomic level. However, the peaks in the NMC-oxalate, which are less sharp than those in $NiC_2O_4.2H_2O$, suggested lower crystal sizes and a fluorescence effect due to the presence of cobalt and manganese atoms [5]. The difference in doping variation lies in the number of wave intensities only. Thus, the addition of metal doping to the material does not cause significant differences in the precursor's crystalline structure.

The group of compounds contained in the precursor sample is seen from the FTIR analysis in Fig. 2. The presence of the O-H group in the precursor sample is indicated by a sharp peak at the wave number of 3340 cm^{-1}, according to the reference that is at the wavelengths of 3300–3500 cm^{-1} and 1600 cm^{-1} [16]. The presence of the O-H group is a representation of the tension vibrations of the water molecular structure (H_2O) on the precursor. In addition, there are also C-O and Ni-O groups on the samples read in the range of 1315 cm^{-1} and 480 cm^{-1}. The result is consistent with the reference, that is, the C-O group is found between the wave number 1300 cm^{-1}[16] and the Ni-O Group at 485 cm^{-1}[17]. The presence of C-O, O-H, and Ni-O groups indicates that the samples made are precursors of nickel oxalate.

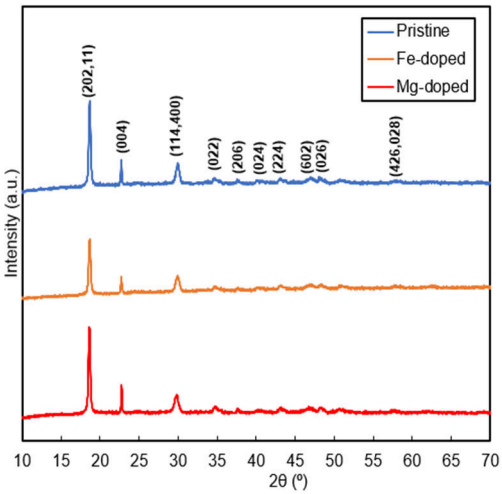

Fig. 1. NMC622 Precursor XRD Results with Fe/Mg Doping

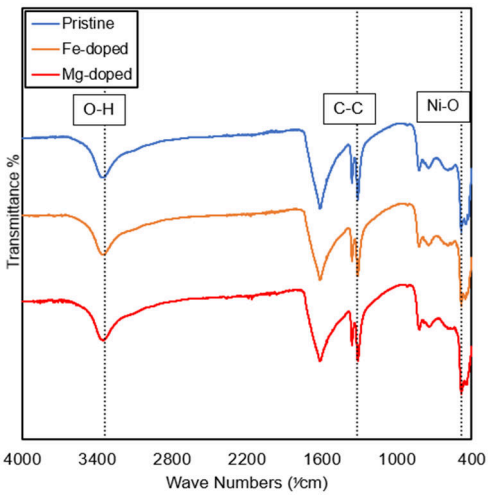

Fig. 2. NMC622 Precursor FTIR Results with Fe/Mg Doping

3.3 Analysis of NMC622 materials

The NMC622 precursor that has been mixed with lithium is then calcinated at a temperature of 500 °C for 6 hours and disintered at 900 °C for 12 hours in a muffle furnace to form the $Li[Ni_{(0,6-y)}Mn_{0,2}Co_{0,2}X_y]O_2$ (X = Fe, Mg; y = 0.01, 0.03, 0.05). It can be seen in Fig 3 that the samples of the NMC622 material that have been made have the same peak number as the commercial NMC which indicates that the material that has been made is a NMC material. The addition of metal doping does not cause XRD results to differ on NMC622. Peaks other than peaks at angles of 20.5-22° indicate the α-$NaFeO_2$ structure with space room group R3m [18]. Peak at an angle of 20.5-22° according to the diffraction (020) and (110) of the Li_2MnO_3 components [1].

From Fig. 3, the coefficient R, parameter value c/a, and intensity ratio can be determined. Calculation of lattice parameters using the following method of square regression

$$n\,\lambda = 2d \sin(\theta) \quad (1)$$

n = the order of the reflection (positive integer)
λ = X-ray wavelength
d = spaing of thee crystal planes
sin (θ) = diffraction angel
θ = the angle between the wavevector of the incident plane wave (°)

$$\frac{1}{d_{hkl}^2} = \frac{4}{3}\left[(h^2 + k^2 + hk) + l^2\left(\frac{a}{c}\right)^2\right]\frac{1}{a^2}\frac{1}{d_{hkl}^2} = \frac{4}{3}\left[(h^2 + k^2 + hk) + l^2\left(\frac{a}{c}\right)^2\right]\frac{1}{a^2} \quad (2)$$

$$\frac{1}{d_{hkl}^2 l^2} = \frac{4}{3}\frac{1}{l^2 a^2}[(h^2 + k^2 + hk) + l^2]\frac{1}{c^2}\frac{1}{d_{hkl}^2 l^2} = \frac{4}{3}\frac{1}{l^2 a^2}[(h^2 + k^2 + hk) + l^2]\frac{1}{c^2} \quad (3)$$

Equation (3) has identical form with regression equation y = mx + n, with :

$$\frac{1}{a_{hkl}^2 l^2}; x = \frac{4}{3}\frac{1}{l^2}(h^2 + k^2 + hk); m = \frac{1}{a^2}; n = \frac{1}{c^2}$$

$$\frac{1}{a_{hkl}^2 l^2}; x = \frac{4}{3}\frac{1}{l^2}(h^2 + k^2 + hk); m = \frac{1}{a^2}; n = \frac{1}{c^2} \quad (4)$$

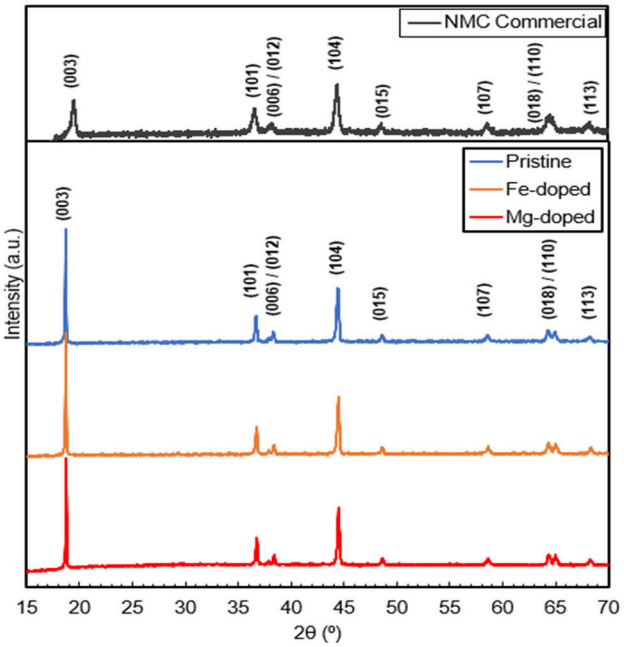

Fig. 3. XRD diffactogram of LiNMC622 and the Fe/Mg doped NMC

From Table 2 all samples have c/a values of more than 4,899. The ideal c/a ratio value on the lattice of the parameter is 4,8989, when the larger value indicates the more orderly layer of material structure and the easier the Li ions to transfer [3]. Commercial NMC have a c/a value of 4.877 so the samples made are higher than the commercial samples. It can also be seen that the addition of metal doping does not have much influence on the value of c/a which explains that Li's transfer ability is the same.

Table 2. Lattice Parameter of NMC 622 Materials

Sample	a (Å)	c (Å)	Lattice Parameter (c/a)	Intensity Ratio (IR)	R coeffisien
NMC Commercial	2.88	14.05	4.88	0.75	0.35
Pristine NMC622	2.8648	14.1705	4.9462	0.4212	0.5022
Fe-doped NMC622	2.8648	14.1705	4.9462	0.4202	0.5007
Mg-doped NMC622	2.8648	14.1705	4.9462	0.4208	0.5007

According to earlier research on Ni-rich cathode materials, the rate of cation mixing will be slower if the intensity ratio (IR) (I(003)/I(004)) is larger. On the other hand, materials have the potential to interact cations if the IR lower than 1,2 [19]. Table 2 shows that the sample's

IR value is lower than that of the commercial NMC. The IR value on the sample with metal doping is slightly smaller than the pristine sample. This suggests that the cation mixing probability of the sample being doped is higher than the pristine [2].
Calcination aims to evaporate components such as oxalate and water that are no longer needed. It can be seen from FTIR analysis results of NMC622 materials in Fig 4 that there is no O-H group in the material that indicates the loss of water on the sample after the process of calcination and sintering as a result of heating. Further on the sample there is a CO_3 group indicated at the wave numbers ~1413 cm^{-1} dan ~804 cm^{-1}. Carbonate clusters are formed due to excess Li and prolonged exposure to air [20]. LiOH can easily be converted to $LiCO_3$ due to the presence of CO in the air and is considered as a detoxifier [5]. The existence of a CO_3 group will affect the performance of the battery produced.

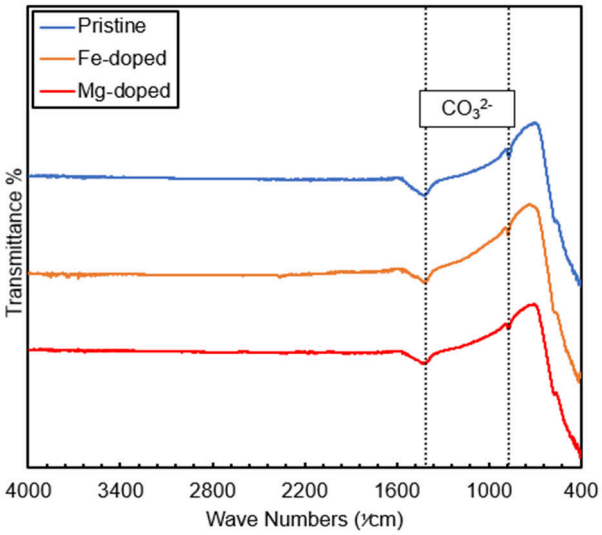

Fig. 4. FTIR Spectra of the pristine LiNMC622 and its modification with Fe/Mg

3.4 Electrochemical Performance on LiNMC622 Cells

The electrochemical performance of the NMC622 materials can be seen from its charge-discharge ability and its cycle stability. As seen from Fig. 5. and Fig. 6., the pristine NMC622 obtained a specific charging capacity of 146.95 mAh/gram. The sample doped with 1 mol% Fe showed the best capacity compared to other Fe variations, where its specific charge capacity was 144.40 mAh/gram and specific discharge capacity 85.87 mAh/gram. However, the capacity of the NMC622 sample doped to Fe was smaller than the pristine's. The low discharge capacity of the Fe-doped sample may be due to the lower release capacity in the rich Ni material and Li-diffusion resistance escalation [21].
The discharge capacity of the 1 mol%, 3 mol%, and 5 mol% Mg-doped sample were respectively 149.70 mAh/gram, 159.25 mAh/gram, 163.04 mAh/gram whereas the discharge capacity were 99.61 mAh per gram, 95.91 mAh /gram, and 84.89 m Ah /gram. All Mg-doped samples have higher specific capacities than pristine NMC samples, which exhibit improved capacity performance. The charge-discharge voltage of the ideal lithium-ion should remain constant during the course of its lifespan [22]. Therefore, the best doping addition variation of Mg is 1 mol%, where the average voltage is 3.63 V. In addition, the discharge capacity of Mg 1 mol% is also higher than the others.

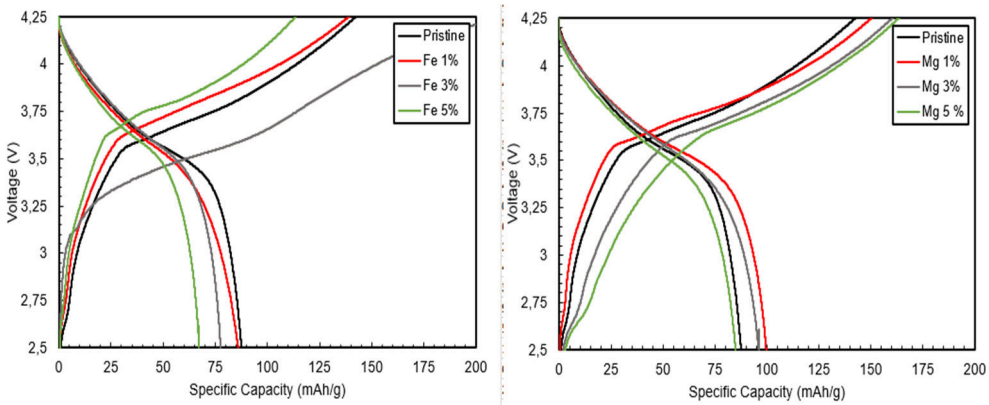

Fig. 5. Voltage Profiles of LiNMC622 Material with Fe Doping in 0,1 C

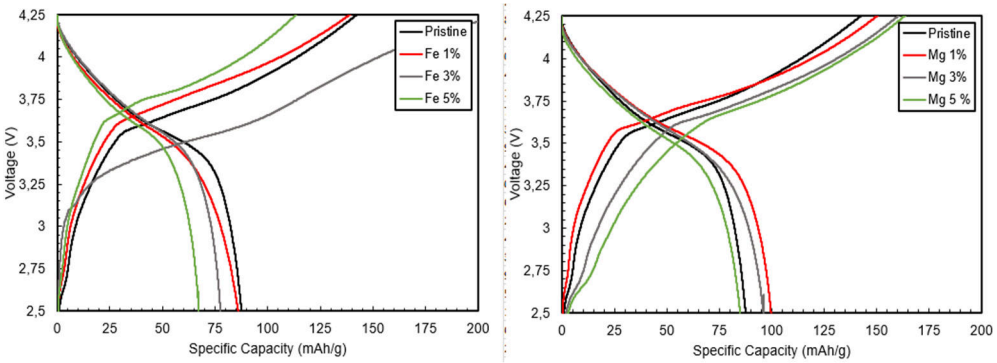

Fig. 6. Voltage Profiles of LiNMC622 Material with Mg Doping in 0,1 C

4 Conclusion

This study successfully employed nickel that was recovered from used nickel catalysts as raw materials for creating the cathode material for the NMC battery. Co-precipitation method was successfully used to create Fe and Mg doped NMC622 cathode active materials, which were then tested for electrochemical performance and the structural effects of the doping. The structural analysis revealed that the doped materials had identical structure to $Li[Ni_{0,6}Mn_{0,2}Co_{0,2}X_y]O_2$ with layered α-$NaFeO_2$-like hexagonal structure. Dopants have an impact on the intensity ratio of lattice parameter, which was thought to be the cause of the observed increased cycle capacity. The electrochemical test resulted among the dopants, Mg 1 mol% showed the best discharge capacity at 99,61 mAh/g. Overall, Mg shown huge potential as a dopant for structurally stable, Ni-rich NMC cathode materials, leading to a greater electrochemical capacity of the Mg-doped cathode material. The functional test of Mg as doping material needs to be further investigated to maximize its utilization for a longer cycle life and thermal stability on lithium ion cathode materials.

Acknowledgment. This research was funded by the Non-APBN Universitas Sebelas Maret fund Hibah Grup Riset (HGR-UNS) A grant no. 228/UN27.22/PT.01.03/2023.

References

1. Q. Li, G. Li, C. Fu, D. Luo, J. Fan, J. Zheng, and L. Li, Electrochim. Acta **154**, 249-258, (2015).
2. A. R. Nurohmah, M. Ayuningtyas, C. S. Yudha, A. Purwanto, and H. Widiyandari, Evergreen **9** (2), pp.427-437, (2022).
3. L. Xu, F. Zhou, J. Kong, H. Zhou, Q. Zhang, Q. Wang, and G. Yan,. Solid State Ionics, **324**, 49. (2018).
4. I. Jung, J. Choi, and Y. Tak, J. Mater. Chem., **20**(29), 6164-6169, (2010)
5. S. S. Nisa, A. R. Nurohmah, C. S. Yudha, H. Nilasary, H. Nursukatmo, E. R. Dyartanti, and A. Purwanto, J. Presipitasi **18**(2), 349–357 (2021)
6. S. S. Nisa, M. Rahmawati, C. S. Yudha, H. Nilasary, H. Nursukatmo, H. S. Oktaviano, S. U. Muzayanha, A. Purwanto, Batteries, **8**, 4, (2022)
7. H. J. Noh, S. Youn, C. S. Yoon, and Y. K. Sun, Journal of power sources, **233**, 121-130. (2013).
8. C. Lu, S. Yang, H. Wu, Y. Zhang, X. Yang, T. Liang, Electrochim. Acta **209** 448–455. (2016).
9. M. Eilers-Rethwisch, M. Winter, and F. M. Schappacher, J. Power Sources **387**, 101-107. (2018).
10. A. L. Lipson, J. L. Durham, M. LeResche, I. Abu-Baker, M. J. Murphy, T. T. Fister, L. Wang, F. Zhou, L. Liu, K. Kim, D. Johnson, ACS Applied Materials & Interfaces, **12**(16), 18512–18518. (2020).
11. S. Park, D. Kim, H. Ku, M. Jo, S. Kim, J. Song, J. Yu, and K. Kwon, Electrochim. Acta, **296** 814–822 (2019).
12. T. Sattar, S. H. Lee, S. J. Sim, B. S. Jin, and H. S. Kim, Int. J. of Hydrogen Energy, **45**(38), 19567-19576, (2020).
13. A. Jihad, A. A. N. Pratama, C. S. Yudha, M. Rahmawati, H. Widiyandari, and A. Purwanto, *Proceedings of the 2021 International Conference on Engineering and Information Technology for Sustainable Industry* (pp. 1-7), (2020).
14. C. Mohanty, S. S. Behera, B. Marandi, S. K. Tripathy, P. K. Parhi, and K. Sanjay, Separation and Purification Technology, **276**, 119377. (2021).
15. R. S. Lakshmi, R. T. Ravindra, R. G. Siva, T. Endo, and R. L. Frost, Spectrochim. Acta Part A: Molecular and Biomolecular Spectroscopy, **123**, 25–29, (2014).
16. A. S. Wijareni, H. Widiyandari, A. Purwanto, A. F. Arif, and M. Z. Mubarok, Energies, **15**(16), 5794. (2022).
17. I. Jung, J. Choi, and Y. Tak, J. Mater. Chem. **20**(29), 6164-6169. (2010)
18. M. Lou, S. S. Fan, H. T. Yu, Y. Xie, Q. Zhang, Y. R. Zhu, et al, J.Alloys and Compounds, **739**, 607-615, (2018).
19. Z. Qiu, Y. Zhang, P. Dong, S. Xia, Y. Yao, Solid State Ionics **307**, 73–78. (2017).
20. O. Haik, N. Leifer, Z. Samuk-Fromovich, E. Zinigrad, B. Markovsky, L. Larush, et al, J. Electrochem. Soc. **157**, A1099. (2010).
21. G. Prado, A. Rougier, L. Fournes, and C. Delmas, J. Electrochem. Soc. **147**(8), 2880, (2000).
22. J. E. Harlow, S. L. Glazier, J. Li, and J. R. Dahn, J. Electrochem. Soc**. 165**(16), A3595. (2018).
23. A. Mecke, I. Lee, J.R. Baker jr., M.M. Banaszak Holl, B.G. Orr, Eur. Phys. J. E **14**, 7 (2004)
24. M. Ben Rabha, M.F. Boujmil, M. Saadoun, B. Bessaïs, Eur. Phys. J. Appl. Phys. (to be published)
25. F. De Lillo, F. Cecconi, G. Lacorata, A. Vulpiani, EPL, **84** (2008)
26. L. T. De Luca, *Propulsion physics* (EDP Sciences, Les Ulis, 2009)